Published in final edited form as:
Neuroscience. 2008 July 31; 155(1): 31–44. doi:10.1016/j.neuroscience.2008.05.028.

Two novel alleles of tottering with distinct Ca(v)2.1 calcium channel neuropathologies

Takafumi Miki[1,*], **Theresa A. Zwingman**[2,*], **Minoru Wakamori**[1], **Cathy M. Lutz**[3], **Susan A. Cook**[3], **David A. Hosford**[4], **Karl Herrup**[5], **Colin F. Fletcher**[6], **Yasuo Mori**[1], **Wayne N. Frankel**[3], and **Verity A. Letts**[3,@]

1*Laboratory of Molecular Biology, Department of Synthetic Chemistry and Biological Chemistry, Graduate School of Engineering, Kyoto University, 615-8510 Kyoto, Japan*

2*Allen Institute for Brain Science, Seattle, Washington 9810.*

3*The Jackson Laboratory, 600 Main Street, Bar Harbor, Maine 04609*

4*Targacept, Inc., 200 East First Street, Winston-Salem, NC 27101-4165*

5*Department of Cell Biology and Neuroscience, Rutgers University, Piscataway, NJ 08854*

6*National Human Genome Research Institute, NIH, Bethesda, MD 20892*

Abstract

The calcium channel *CACNA1A* gene encodes the pore-forming, voltage-sensitive subunit of the voltage-dependent calcium Ca(v)2.1 type channel. Mutations in this gene have been linked to several human disorders, including familial hemiplegic migraine, episodic ataxia 2 and spinocerebellar ataxia type 6. The mouse homologue, *Cacna1a*, is associated with the tottering, *Cacna1a*^{tg}, mutant series. Here we describe two new missense mutant alleles, *Cacna1a*$^{tg\text{-}4J}$ and *Cacna1a*$^{Tg\text{-}5J}$. The *Cacna1a*$^{tg\text{-}4J}$ mutation is a valine to alanine mutation at amino acid 581, in segment S5 of domain II. The recessive *Cacna1a*$^{tg\text{-}4J}$ mutant exhibited the ataxia, paroxysmal dyskinesia and absence seizures reminiscent of the original tottering mouse. The *Cacna1a*$^{tg\text{-}4J}$ mutant also showed altered activation and inactivation kinetics of the Ca(v)2.1 channel, not previously reported for other tottering alleles. The semi-dominant *Cacna1a*$^{Tg\text{-}5J}$ mutation changed a conserved arginine residue to glutamine at amino acid 1252 within segment S4 of domain III. The heterozygous mouse was ataxic and homozygotes rarely survived. The *Cacna1a*$^{Tg\text{-}5J}$ mutation caused a shift in both voltage activation and inactivation to lower voltages, showing that this arginine residue is critical for sensing Ca(v)2.1 voltage changes. These two tottering mouse models illustrate how novel allelic variants can contribute to functional studies of the Ca(v)2.1 calcium channel.

Keywords

tottering alleles; Ca(v)2.1 calcium channels; semi-dominant mutation

@Corresponding author: Verity A. Letts, The Jackson Laboratory, 600 Main Street, Bar Harbor, Maine 04609. Email: verity.letts@jax.org.
*These authors contributed equally to this study.
Section editor: Dr. C Sotelo

Introduction

Voltage-dependent calcium channels allow the entry of calcium ions into the cell when the membrane is depolarized, triggering multiple downstream events including synaptic vesicle activation, neuronal plasticity and gene transcription (Catterall, 2000). Electrophysiological and pharmacological studies have defined several types of calcium channels in neurons, including the Ca(v)2.1 or P/Q-type channels. The major structural alpha subunit of this calcium channel includes the voltage-sensing and ion-gating functions encoded by the *CACNA1A* gene. The Ca(v)2.1 channel predominantly functions in neurotransmitter release at central synapses (Wheeler et al., 1994; Qian and Noebels, 2000) (Wu et al., 1999) and neuromuscular junctions (Uchitel et al., 1992).

Mutations in the *CACNA1A* gene in humans have been associated with familial hemiplegic migraine with aura (FHM) (Pietrobon and Striessnig, 2003) (Alonso et al., 2004), episodic ataxia type 2 (EA2) (Spacey et al., 2004) (Cricchi et al., 2007) (Guida et al., 2001), spinocerebellar ataxia type 6 (SCA6) (Zhuchenko et al., 1997) (Lindquist et al., 2006) (Pulst et al., 2005) (Shimazaki et al., 2001) and epilepsy (Jouvenceau et al., 2001) (Beauvais et al., 2004). SCA6 often arises from a triplet expansion in the glutamate repeat at the carboxy terminus, whereas the EA2 mutations range from missense, nonsense, splice site or deletion mutations (Ophoff et al., 1996; Kraus et al., 2000). Reduced or absent Ca(v)2.1 channel activity is often associated with EA2 mutations (Guida et al., 2001) (Spacey et al., 2004) (Jeng et al., 2008). FHM mutations arise from missense mutations; in *most* cases the Ca(v)2.1 channels are activated at more hyperpolarized potentials (Tottene et al., 2002; Pietrobon and Striessnig, 2003; Mullner et al., 2004) and sometimes a reduced density of calcium channels is observed (Hans et al., 1999) (Barrett et al., 2005). From studies of the mouse mutations tottering (*Cacna1a*^{tg} or *tg*), leaner (*Cacna1a*$^{tg\text{-}la}$) (Ayata et al., 2000) and a mouse strain carrying a human FHM mutation (van den Maagdenberg et al., 2004), the CACNA1A gene has also been implicated in cortical spreading depression (CSD). CSD is believed to underlie the aura symptoms associated with migraine.

The FHM and EA2 human mutations are inherited in a dominant manner. In contrast, the rodent models with mutations in the *Cacna1a* gene are predominantly recessive, with only one dominant mutation recently described in the wobbly mouse (Xie et al., 2007). The tottering and leaner mutants were the first *Cacna1a* mouse mutants to be characterized. The tottering mouse is relatively mildly affected with ataxia, paroxysmal dyskinesia and absence seizures (Noebels and Sidman, 1979) (Fletcher et al., 1996), whereas the leaner mouse is far more severe; the mice are runted with cell loss in the cerebellum and early death (Herrup and Wilczynski, 1982). The two *Cacna1a* targeted mutations are phenotypically similar to the leaner mutation (Jun et al., 1999; Fletcher et al., 2001), and additional missense mutations, including rolling Nagoya (Mori et al., 2000) and rocker (Zwingman et al., 2001), all show the ataxia observed in the tottering mouse. A newly described ataxic model in rats, groggy, is also a recessive mutant (Tokuda et al., 2007).

We describe here the histology and neurophysiology of two new spontaneous mutations in the *Cacna1a* gene; the semi-dominant mutation in *Tg-5J* and a recessive mutation in the *tg-4J* allele. These two mutations illustrate how novel missense mutations can validate and further define functional regions within large ion channel subunits like the CACNA1A protein.

Experimental Procedures

Identification of the spontaneous ataxic strains

The *Cacna1a*$^{tg\text{-}4J}$ mutant was first detected in the C3H/HeJ colony of Dr. Edward Birkenmeier at The Jackson Laboratory in 1996. It is now maintained as a congenic B6.C3H-

Cacna1a$^{tg\text{-}4J}$ (*tg-4J*) strain. The *Cacna1a*$^{Tg\text{-}5J}$ (*Tg-5J*) strain arose in the B10.M-*H2*^{f}/nMob *Fmn1*$^{ld\text{-}2J}$/J strain in 1995 and is now on the C57BL/10 (B10) background and on a mixed background between B10 and BALB/cByJ. All animals are housed at The Jackson Laboratory (Bar Harbor, ME), regulated by the Animal Care and Use Committee. The mice were provided a commercial diet and water *ad libitum* under conventional conditions with controlled temperature, humidity, and lighting.

cDNA cloning and sequence analysis

cDNAs encoding the CACNA1A subunit were isolated by reverse transcriptase-polymerase chain reaction methods (RT-PCR) using the random primer DNA labeling system (Life Technologies, Grand Island, NY) and total RNA isolated from mouse brain. PCR primers were designed according to the published sequence data (Fletcher et al., 1996) such that the entire 6495 bp sequence was covered. RT-PCR products were subcloned using the TOPO TA Cloning Kit (Life Technologies, Grand Island, NY), and sequenced using an automated sequencer (ABI prism model 377; Applied Biosystems, Foster City, CA). Sequence information was obtained separately from four mutants and three background control mice for each allele studied. The results were confirmed by genomic DNA sequencing.

Immunohistochemistry

Animals were deeply anesthetized with tribromoethanol and transcardially perfused with 4% paraformaldehyde in 0.1M phosphate buffer (pH 7.5). The brains were immediately removed from the cranium and fixed for an additional 4 hr at 4°C. The brains were then cryoprotected in 18% (w/v) sucrose in PBS at 4°C overnight. Samples were embedded in OCT, 10 micron cryostat sections were cut and allowed to air dry on gelatin coated slides.

Tissue were processed for immunohistochemistry with the anti-tyrosine hydroxylase and calbindin antibodies, as previously described (Zwingman et al., 2001). To evaluate the immunostaining between animals, digital images were captured at defined exposure times.

Green Fluorescent protein (GFP) labeling of Purkinje cells

Tg-5J heterozygous mice from the mixed B10;BALB background were intercrossed to a B6 mouse strain carrying a transgene with the parvalbumin promoter fused to the green fluorescent protein (GFP) gene (strain # B20) (Chattopadhyaya et al., 2004). Brains from F2 homozygous *Tg-5J* and controls were dissected at 24 days of age for fixation in Z-fix buffer (Anatech, MI) for 3–4 hours. Vibrotome sagittal sections (60–100um) were mounted onto slides with Clear-mount (Zymed, CA). The sections were viewed using a Leica SP5 AOBS spectral confocal microscope, with a 63X, 1.3 NA glycerol immersion objective. Excitation was at 488nm, with emission collection optimized for green fluorescence detection.

Golgi-Cox

Mutant and control animals were euthanized by carbon dioxide asphyxiation and their brains removed and immersed in fixative (10 mg/ml potassium dichromate, 10 mg/ml mercuric chloride, and 4.5 mg/ml potassium chromate; any precipitate was cleared by acidification with 0.1N HCl). The brains were stored in the dark undisturbed for 6–8 weeks before dehydration, infiltration with low viscosity nitrocellulose celloidin/parlodion (Fisher, PA) and hardened with chloroform vapors (Zwingman et al., 2001). The blocks were sectioned and mounted onto slides as previously described (Zwingman et al., 2001).

Electrocorticographic Recordings

Silver wire electrodes (0.125 mm diameter) soldered to a microminiature connector were implanted bilaterally into the subdural space over frontal and parietal cortex of anesthetized

mice several days prior to recording (Noebels and Sidman, 1979). Cortical activity was recorded from mutants and controls moving freely in the test cage for prolonged periods. Ethosuximide (Sigma, MO), an inhibitor of absence seizure activity, was injected (150 mg/kg, i.p.) to confirm that the seizure activity was suppressed.

Construction of expression plasmids encoding Ca2+ channel CACNA1A subunit with Tg-5J or tg-4J mutations

For construction of expression cDNA encoding the *Tg-5J -CACNA1A* (BI-2) subunit mutant, a PCR fragment was amplified using pSPCBI-2 (Mori et al., 1991) as a template, a primer BIPMI(+) (5'-ACCACACCGTGGTCCAAGTGAACAAAAATG-3') (sense) and a primer 5J (−) (5'-GTAGCACCTGGAGCACTCGGAGGGATTTG-3') (antisense). A PCR fragment amplified using pSPCBI-2, and a primer 5J(+)(5'-CAAATCCCTCCGAGTGCTCCAGGGTGCTAC-3') (sense) and a primer BIAcI(−)(5'-GAAGTAGACCACGTAGAAGATGGACATCTC-5') (antisense), were combined with the primers BIPMI(+) and BIAcI(−) in the subsequent PCR. The PCR product was digested with *Pfl*MI and *Acc*I, and the yielded mouse fragment was substituted for the corresponding *Pfl*MI (3574)/*Acc*I (4506) sequence of the rabbit CACNA1A (BI-2) cDNA in the recombinant plasmid pK4KBI-2 (Niidome et al., 1994) to obtain pK4KBI-*Tg-5J*.

The construction of expression cDNA encoding the *tg-4J -CACNA1A* (BI-2) subunit mutant started with the PCR fragment amplified using pSPCBI-2 as a template, a primer BIXhI(+) (5'-GTGCCAAGCTGGAGAACTCGAGTTTTTTCC-3')(sense) and a primer 4J(−) (5'-CCCCAGAAGTGCAAAGGCAACGATAAACAG-3')(antisense). A PCR fragment amplified using pSPCBI-2, and a primer 4J(+) (5'-CTGTTTATCGTTGCCTTTGCACTTCTGGGG-3') (sense) and a primer BIHnIII(−) (5'-CTTCTGCAGGGCAAGCTTTTGATTGACGGC-5') (antisense), were combined with the primers BIXhI(+) and BIHnIII(−) in the subsequent PCR. The PCR product was digested with *Xho*I and *Hin*dIII, and the yielded mouse fragment was substituted for the corresponding *Xho*I (1396)/ *Hin*dIII (2210) sequence of the rabbit *CACNA1A* (BI-2) cDNA in the recombinant plasmid pK4KBI-2 (Niidome et al., 1994) to obtain pK4KBI-tg-4J.

Expression of recombinant CACNA1A $Ca2^{+}$ channels with Tg-5J or tg-4J mutations in BHK cells

BHK cells were transfected with the pAGS-3 recombinant plasmid pAGS-3a2 (Klöckner et al., 1995) and pCABE (Niidome et al., 1994) using the CaPO4 protocol (Chen and Okayama, 1987), and were cultured in Dulbecco's modified Eagle medium (DMEM) containing G-418 (600 μg/ml) (Gibco BRL, Gaithersberg, MD), to first establish a BHK line, BHK6, with stable expression of the CACNB1b and CACNA2D subunits. To transiently express the wild-type CACNA1A channel, the *Tg-5J* mutant CACNA1A channel or the *tg-4J* mutant CACNA1A channel, BHK6 cells were transfected with the recombinant plasmid pK4KBI-2, pK4KBI-*Tg-5J* or pK4KBI- *tg-4J*, plus pH3-CD8 containing the cDNA of the T-cell antigen CD8 (Jurman et al., 1994). Transfection was carried out using Effectene Transfection Reagent (QIAGEN, Hilden, Germany). Cells were trypsinized, diluted with Dulbecco's modified Eagle's medium (DMEM) containing10% fetal bovine serum (FBS), 30 units/ml penicillin, and 30 μg/ml streptomycin, and plated onto culture dishes (Primaria #3801, Nippon Becton Dickinson, Tokyo, Japan) 18 h after transfection. Then cells were subjected to measurements 48–66 h after the plating. Cells expressing Ca(v)2.1 channels were selected through detection of CD8 coexpression using polystyrene microspheres precoated with antibody to CD8 (Dynabeads M-450 CD8;DYNAL, Oslo, Norway).

Preparation of dissociated Purkinje cells

Purkinje cells were freshly dissociated from 14- to 26-day old mice. The procedure for obtaining dissociated cells from mice is similar to that described elsewhere (Wakamori et al., 1993). Coronal slices (350-μm-thick) of cerebellum were prepared using a microslicer (Leica, Nussloch, Germany; VT-1000S). After preincubation in Krebs' solution for 46 min at 31 C, the slices were digested: first in Krebs' solution containing 0.025% pronase (Calbiochem-Nocabiochem, La Jolla, CA) for 23 min at 31 C and then in solution containing 0.025% thermolysin (type X; Sigma, MO) for 23 min at 31 C. The Krebs' solution used for preincubation and digestion contained the following (in mM): 124 NaCl, 5 KCl, 1.2 KH_2PO_4, 2.4 $CaCl_2$, 1.3 $MgSO_4$, 26 $NaHCO_3$, and 10 glucose. The solution was continuously oxygenated with 95% O_2 and 5% CO_2. Then the brain slices were punched out and dissociated mechanically by the use of fine glass pipettes having a tip diameter of 100–200 μm. Dissociated cells settled on tissue culture dishes (Primaria #3801; Nippon Becton Dickinson, Tokyo, Japan) within 30 min. Purkinje cells were identified by their large diameter and characteristic pear shape because of the stump of the apical dendrite. To make a sufficient space-clamp of the Purkinje cell body, Purkinje cells lacking most of dendrites were used throughout the present experiments.

Whole-cell recordings

Electrophysiological measurements were performed on BHK and Purkinje cells. Currents were recorded at room temperature (22 – 25 °C) using whole-cell mode of the patch-clamp technique (Hamill et al., 1981) with an EPC-9 patch-clamp amplifier (HEKA, Darmstadt, Germany). Patch pipettes were made from borosilicate glass capillaries (1.5mm outer diameter; Hilgenberg, Malsfeld, Germany) using a model P-87 Flaming-Brown micropipette puller (Sutter Instrument Co., San Rafael, CA). The patch electrodes were fire-polished. Pipette resistance ranged from 2 to 4 MOhm when filled with the pipette solutions described below. The series resistance was electronically compensated to >50 % and both the leakage and the remaining capacitance were subtracted by −P/4 method. Currents were sampled at 100 kHz after low pass filtering at 8.4 kHz in the experiments of activation kinetics, otherwise sampled at 20 kHz after low pass filtering at 2.9 kHz. Stimulation and data acquisition were performed using the PULSE program (version 7.5, HEKA Elektronik, Lambrecht, Germany). Ba^{2+} currents were recorded in an external solution that contained (in mM): 3 $BaCl_2$, 155 tetraethylammonium chloride (TEA-Cl), 10 HEPES, 10 glucose (pH adjusted to 7.4 with TEA-OH). The pipette solution contained (in mM): 85 Cs-aspartate, 40 CsCl, 2 $MgCl_2$, 5 EGTA, 2 ATPMg, 5 HEPES, 10 creatine-phosphate (pH adjusted to 7.2 with CsOH).

Statistical comparison between normal and mutant channels was performed by Student's t test (*, $P < 0.05$; **, $P < 0.01$; ***, $P < 0.001$).

Results

Genetic analysis of two new spontaneous mouse mutants with ataxia

A spontaneous mouse mutant with an ataxic gait arose in the C3H/HeJ colony. The phenotype was recessive and, along with the associated dyskinesia, was reminiscent of the previously described tottering (*Cacna1a*^{tg}) mouse. A complementation cross to tottering mice confirmed that this mutant was a new allele of tottering and it was renamed *Cacna1a*$^{tg\text{-}4J}$ (referred to as *tg-4J* throughout this paper).

A second ataxic mouse mutant arose in the B10.M-H2^{f}/nMob Fmn1$^{ld\text{-}2J}$/J colony. The ataxia appeared to be inherited in a dominant fashion. To genetically map this mutation, affected mice from this strain were backcrossed to CAST/EiJ mice to produce the second backcrossed (N2) generation. Analysis of 124 N2 animals revealed tight linkage of the mutant locus to markers

on Chromosome 8, including the *Cacna1a* locus. A complementation test between the heterozygous animals and heterozygous leaner (*Cacna1a*$^{+/tg\text{-}la}$) animals showed that the putative compound heterozygote animals is ataxic and had a tendency to lean to one side. This result indicated that this new mutation was indeed allelic with leaner. The new mutation is known as *Cacna1a*$^{Tg\text{-}5J}$ (referred to as *Tg-5J*).

Identification of the 2 missense mutations

From analysis of the RNA and DNA from the *tg-4J* mutant, a single nucleotide change distinguished *tg-4J* from the chromosome of origin (C3H/HeJ); a T-to-C transition at nucleotide residue 1742 (Fig. 1). This alteration predicts a conservative amino acid substitution, changing valine to alanine at position 581 (Val581Ala). This valine is located in the transmembrane region S5 in the second homologous domain (Fig. 1).

Likewise, sequence analysis from the *Tg-5J* strain revealed a single nucleotide change (G3755A) in domain III that encodes a charge-neutralizing amino acid substitution (Arg1252Gln) (Fig. 1). Importantly, the mutated arginine is one of the highly conserved positively charged amino acids located at every third position in the voltage-sensing region S4 in many ion-gating channels, including many voltage-dependent calcium channels as well as low voltage calcium and sodium channels as illustrated in Fig. 2. Interestingly, the only other dominant mouse mutation, wobbly, that has been reported also has a missense mutation in a nearby arginine residue, three amino acids downstream at position 1255, in the same S4 segment of domain III (Xie et al., 2007).

Behavior and viability of the new tottering mice

Both the homozygous *tg-4J* and heterozygous *Tg-5J* mutants displayed an ataxic gait, suggestive of cerebellar dysfunction. However the ataxia in *Tg-5J* was subtly different from the uncoordinated gait in tottering and *tg-4J* mice. Both of these mutants had an ataxic gait with pronounced high-stepping, waggling movements. In the heterozygous *Tg-5J* mutant, the hind limbs were splayed laterally from the body and the gait was noticeably shakier than tottering. Additionally, the paroxysmal dyskinesia phenotype was observed in the *tg-4J* homozygote but not the *Tg-5J* heterozygote mutants. The *Tg-5J* allele is semi-dominant as the heterozygous *Tg-5J* mice were less affected than the *Tg-5J* homozygotes.

In contrast to the recessive *tg-4J* homozygotes that had a normal lifespan and were able to breed, the *Tg-5J* homozyygotes were runted, severely ataxic, and died before 6 weeks of age. This was particularly noticeable for the *Tg-5J* mutants on the B10 isogenic background where, in order to maintain the mutation, heterozygous (het) to wild-type matings were favored as most het by het matings produced no offspring. We also established crosses between the B10.*Tg-5J* and the BALB/cByJ inbred strain. First generation hybrids routinely show increased vigor, and this proved to be true for the *Tg-5J* mutants. B6:BALB het by het *Tg-5J* matings successfully produced litters, but only 3% of the offspring could be confirmed as being homozygous for the *Tg-5J* mutation. These pups also did not survive beyond 6 weeks of age.

To maintain background uniformity, all the *tg-4J* results presented here came from mice on the B6 background and all the *Tg-5J* results were from the B10 background, with one exception for the green fluorescent protein studies.

Brain cytoarchitecture and cerebellar morphology appear grossly normal

Our initial pathology studies of the *tg-4J* homozygotes and *Tg-5J* heterozygote mice involved gross histological examination of the central nervous system, with serial sagittal sections through the whole brain. The cytoarchitecture of the mutant brains appeared normal at 2– 4 months of age. We further examined the hippocampus and the cerebral cortex in these mice

by cresyl violet staining and Golgi impregnations. Both areas were indistinguishable from wild-type animals.

We investigated the cerebellum more closely to explain the ataxia observed in these mutants. We found a normal cerebellar morphology and cytoarchitecture in the *tg-4J* homozygotes, *Tg-5J* heterozygotes and even the *Tg-5J* homozygotes compared to wild type. Measurements of the molecular layer width and total area revealed no significant difference between affected and non-affected littermates. Particular attention was paid to the anterior vermis of the cerebellum where severe Purkinje cell loss has been noted in leaner mice (Herrup and Wilczynski, 1982). Western analysis showed no reduction in the amount of CACNA1A protein in brains from either mutant (results not shown).

Calbindin staining and tyrosine hydroxylase expression reveal cerebellar defects

We examined cerebellar sections of *tg-4J* homozygotes, *Tg-5J* heterozygotes and littermate control animals. No reduction in the calbindin staining was observed in the cerebellums from *tg-4J* homozygote and *Tg-5J* heterozygote mice, and no gaps in the Purkinje cell layer were evident (Fig. 3 A, B, C). However we did observe axonal swellings in the Purkinje cells of the mutants, reminiscent of other tottering alleles (Fig. 3) (Rhyu et al., 1999a; Rhyu et al., 1999b).

Tyrosine hydroxylase (TH) is a key enzyme in the noradrenergic biosynthesis pathway. TH expression is normally expressed transiently in a subset of cerebellar Purkinje cells and is not detected after postnatal day 40. Previous studies of tottering, Wobbly and leaner mutant mice have shown persistent expression of TH (Austin et al., 1992) (Xie et al., 2007). We examined normal *tg-4J* homozygotes and *Tg-5J* heterozygotes at 3 months of age and observed expression of TH in both mutants (Fig. 4 C, D, E, and F).

Aberrant branching of the Purkinje cells in the Tg-5J mutant

We further investigated the architecture of the Purkinje cells. To study the homozygous *Tg-5J* mutation, we intercrossed *Tg-5J* heterozygous mice (from the B10xBALB cross) with the B20 strain carrying a transgene expressing the green fluorescent protein (GFP) gene (Chattopadhyaya et al., 2004). Confocal microscopy revealed that the GFP-stained Purkinje cells in the F2 homozygous mutant showed considerably less branching than the control littermate at the same age (Fig. 5). The primary branches had novel, GFP negatively-stained vacuoles that did not impede cytoplasmic flow as we detected GFP protein staining throughout the arbor (Fig. 5 B,C). Vacuoles have previously been reported in the Purkinje cell bodies of SCA1 transgenic mice (Clark et al., 1997), but this is the first report of vacuoles in dendritic branches.

We turned to Golgi impregnation to evaluate both *tg-4J* homozygous and *Tg-5J* heterozygous mice at over a year old. Previous studies of older rocker ($Cacna1a^{rkr}$) mutants revealed a process of Purkinje cell dendritic atrophy that resulted in a thinning of the dendritic mass with unusual terminal dendritic extensions (Zwingman et al., 2001). These extensions often turned and grew back towards the Purkinje cell layer giving the dendritic arbor a weeping willow appearance. During normal aging, the controls in our study underwent a slight reduction in the branching complexity of the Purkinje cell dendritic arbor (Fig. 6 A and B). By contrast, age-matched *Tg-5J* heterozygote animals displayed a Purkinje cell arbor that was significantly reduced in complexity and overall dendritic mass (Fig. 6 E and F). In addition, we observed an abnormal serpentine-like appearance in the tips of the distal dendrites (Fig. 6 E arrow). The shafts of main Purkinje dendrites also show a thickening in the upper molecular layer. In contrast, the *tg-4J* homozygote appeared to have a slight thickening of the secondary dendrites but no other histopathology (Fig. 6 C and D).

Only *tg-4J* showed absence seizures

Another phenotype associated with tottering is absence seizures, observed as characteristic 5–7 Hz spike wave discharges in electroencephalographic (EEG) recordings. EEG studies revealed spike wave discharges, accompanied by behavioral arrest, in *tg-4J* homozygous mice, lasting up to 1.8 seconds in duration and occurring on average 4 times per hour (n=9, total recording time 18.3 h). This is a less profound seizure phenotype than the original tottering mouse with seizures lasting as long as 10 seconds and recurring hundreds of times per day (Noebels and Sidman, 1979). The *tg-4J* mutant seizures were abolished by treatment with the anti-epileptic drug, ethosuximide. We were unable to test *Tg-5J* homozygotes because of their early lethality, but the *Tg-5J* heterozygous animals showed no spike wave discharge activity (n=4).

Calcium channel electrophysiology is altered in both mutations

To determine the functional impact of the mutations on calcium channel activity we initially analyzed recombinant protein transiently expressed in BHK cells. We introduced the T1742C (*tg-4J*) and G3755A (*Tg-5J*) mutations at the corresponding sites of the rabbit *CACNA1A* cDNA (Mori et al., 1991). The control wild-type and mutant cDNAs were inserted in the pK4K plasmid (Niidome et al., 1994) and were transiently expressed in the BHK6 cells, which stably express the CACNA2D and CACNB1b subunits (Wakamori et al., 1998). When membrane potential was stepped from a holding potential (V_h) of −100 mV to a test pulse of 0 or 10 mV the average peak current densities for the *Tg-5J* and *tg-4J* channels were not significantly different from the wild-type channel in a solution containing 3 mM Ba^{2+} (Fig.7 Aa–c). Current-voltage (I–V) relationships for the wild-type and mutant Ba^{2+} currents indicated that the wild-type and mutant channels were activated by step depolarization above −50 mV (*Tg-5J*) or −40 mV (*tg-4J*, wt) from a V_h of −100 mV (Fig. 7, Aa–c). The current amplitude increased with increments of depolarization, reaching peaks in the I–V relationships around 0 (*tg-4J*, wt) and −10 mV (*Tg-5J*) (Fig. 7B). Current amplitudes and densities were not significantly different among wild-type and mutant channels (Fig. 7C) and the capacitance-current relationships were directly proportional.

The activation curves, obtained by fitting peak of tail currents at the fixed potential of −60 mV after 5 msec step depolarization from −50 to 35 mV with 5 mV increments with a single Boltzmann function, showed different voltage dependences between the wild type and mutant channels (Fig. 8 A, B). Specifically, the midpoint of the activation was −27.3 ± 0.6 mV for *Tg-5J* (n = 7, $p = 4.83^{-7}$ v. wt), −14.5 ± 1.0 mV for wt (n = 5) and − 7.0 ± 1.6 mV for *tg-4J* (n = 6, $p = 0.0051$ v. wt) (Table 1). Furthermore, the slope factor (k) was significantly different for 4J: 7.7 ± 0.4 mV for *tg-4J* and 5.1 ± 0.5 mV for wt ($P = 0.0016$). Activation time constants were obtained from single-exponential fits of the activation phase during 5 msec depolarizing steps (Fig. 8 B). *tg-4J* channels showed significantly different τ_a at −25 and −20 mV. Thus, *Tg-5J* has a significant hyperpolarizing shift in voltage dependence indicating that these channels required weaker depolarization for activation compared to the control (Table 1). In contrast, in the *tg-4J* Ca^{2+} channel the activation curve was significantly shifted to depolarizing direction and showed reduction of slope (Fig. 8A and Table 1). Furthermore, the *tg-4J* channel showed accelerated activation speed, unlike the *Tg-5J* channel whose kinetic properties were similar to those of wild-type channel (Fig. 8B).

The voltage dependence of inactivation was determined by the use of 2 sec prepulses to a series of different potentials (−120 to 10 mV), followed by a 20 msec test pulse to 0 (*tg-4J*, wt) or −10 mV (*Tg-5J*). Test current amplitudes were normalized to the peak current amplitude induced by the test pulse of −120 mV and were plotted against the prepulse potentials (Fig. 9A). The inactivation potential midpoint and the slope factor of the inactivation curves fitted by a Boltzmann equation were −63.1 ± 1.9 mV and 6.3 ± 0.6 mV (n = 6) for wt, −79 ± 1.8 mV

(n = 5, p = 0.00017) and 8.6 ± 0.6 mV (p = 0.026) for *Tg-5J* and −61 ± 2.9 mV and 7.7 ± 0.3 mV (n = 5) for *tg-4J* (Fig. 9A). The *Tg-5J* channels required weaker depolarization for inactivation, but the *tg-4J* inactivation curve was indistinguishable from the control (Table 1).

The mean inactivation time currents, τ_{fast} and τ_{slow}, were derived by fitting a sum of two exponential functions to the current decay and were plotted as a function of test potentials from −20 to 0 mV (Fig. 9B). *tg-4J* showed significantly different τ_{fast} at −20 and −10 mV. The fraction of current for each component (fast, slow, and sustained) was plotted as a function of the test potential (for −20 to −10 mV) (Fig. 9C). Overall, the *tg-4J* channel significantly differed from control in inactivation kinetics: the fast component of current decay showed increased fraction but reduced speed in the *tg-4J* channel (Fig. 9B and C).

In previous studies it has been suggested that results from transfected BHK cells may be unreliable due to the aberrant expression of the transgene (van den Maagdenberg et al., 2004) and the reconstruction of calcium channel activity with regulatory subunits that may not reflect the *in vivo* situation. To address these concerns, we investigated Ca(v)2.1 recordings from dissociated Purkinje cells from the mutants and wild-type mice (Fig. 10 and Table 1). Unfortunately we were unable to include the *Tg-5J*/ *Tg-5J* homozygotes in this analysis because of their poor viability.

There is a shift of both the Ca(v)2.1 *Tg-5J*/+ and *tg-4J /tg-4J* activation curves (Fig. 10D, Table 1). From the inactivation curve, the *Tg-5J* heterozygote also shows a shift to lower voltages (Figs. 10E). Both of these shifts are significantly less pronounced in the Purkinje cells from the Tg-5J/+ heterozygotes compared to the BHK results (Table 1). This is expected as the BHK cells have only the *Tg-5J* mutant form of the CACNA1A protein, whereas the Purkinje cells are derived from the *Tg-5J* heterozygous mice that retain one normal copy of the *Cacna1a* gene.

Noticeably both the current amplitude and capacitance are reduced in the *tg-4J* /*tg-4J* homozygote Purkinje cells (Fig. 10C). These differences are attributable to the smaller size of the *tg-4J /tg-4J* Purkinje neuron cell bodies compared to the controls, indicating that the *tg-4J* mutation disrupts not only the function of the Ca(v)2.1 channels but also the cellular development of Purkinje cells. Similar results were observed in the tottering rolling Nagoya allele (Mori et al., 2000). However in contrast to rolling Nagoya, the current density for the *tg-4J* homozygote was not reduced in either the Purkinje or BHK cells (Fig. 7, Fig. 10).

Discussion

These two new spontaneous alleles of tottering reveal an intriguing contrast between the underlying mutations and the phenotypic expression. The *Tg-5J* mutation is due to the loss of a highly conserved arginine residue in a critical voltage-sensing region, with predictably severe consequences. The mutation is semi-dominant, resembling the many human mutations on the CACNA1A gene and the wobbly mouse mutation, with accompanying changes in both the activation and inactivation kinetics of the Ca(v)2.1 channel. In contrast the *tg-4J* mutation is a relatively benign valine to alanine change in the transmembrane S5 region of domain II; one that would not have been predicted to result in a phenotype as pronounced as the previously described recessive tottering alleles.

The *tg-4J* mutation is phenotypically very similar to the original tottering mutation, with ataxia, paroxsymal dyskinesia and absence seizures. The mutant also showed continued tyrosine hydroxylase expression and Purkinje cell axon swelling. Many of the tottering alleles, including *tg-4J*, are recessive as the heterozygous mice are overtly normal. In contrast, the *Tg-5J* allele is semi-dominant with an ataxic gait, but lacking the dyskinesia and absence seizures of the other tottering alleles. Although the *Tg-5J* homozygote rarely survived to 6 weeks of age, we

were able to observe a significant reduction in Purkinje cell dendritic branching in these mice on a mixed genetic background. Persistent tyrosine hydroxylase activity, Purkinje cell axon swelling and branching defects were also observed in the more robust *Tg-5J* heterozygote.

The *Tg-5J* mutation changes a highly conserved arginine residue in S4 of domain III to a glutamine. The arginine is one of 3 in a repeated triplet motif, found not only in the voltage-sensor paddle of calcium channels but also sodium and potassium ion-gated channels (Ruta et al., 2005). Missense mutations that replace the arginine residues have been shown to alter calcium channel function; illustrated by two studies of FHM mutations, one involving the arginine to glutamine mutation in domain I (R192Q) and the second, the R583Q missense mutation in domain II of the *CACNA1A* gene. The R192Q mutation was first reported to cause an increase in calcium current density (Hans et al., 1999), whereas the R583Q mutation showed a shift to more negative potentials for both calcium channel activation and inactivation (Kraus et al., 2000). The R192Q mutation was further studied in a Knock-in mouse strain expressing this human mutation in place of the normal *Cacna1a* mouse gene (van den Maagdenberg et al., 2004). Unlike the many tottering alleles including *tg-4J* and *Tg-5J*, the Knock-in mouse had a normal gait (Kaja et al., 2005). This strain also showed increased susceptibility to cortical spreading depression (CSD), associated with the neurological aura symptoms of migraines. A shift in the calcium channel activation to lower voltages was observed with this mutant that would predictably lead to an increased action potential-evoked calcium influx and increased glutamate release, triggering the CSD response (van den Maagdenberg et al., 2004).

The hyperpolarizing shifts observed in the R192Q and R583Q mutations mirrored our *Tg-5J* results of a negative shift in the calcium channel activation curve. Furthermore we found that *Tg-5J* also had a more hyperpolarized inactivation response. From these results we conclude that this mutation represents a dominant gain-of-function, and we predict that *Tg-5J* will show enhanced Ca(v)2.1 channel activity and increased intracellular calcium concentration in response to depolarizing potentials. However, this enhancement may occur only when the membrane is depolarized from sufficiently hyperpolarized resting potential, since the voltage dependence of inactivation is also shifted to hyperpolarizing potentials by the *Tg-5J* mutation.

The *tg-4J* mutation shifted the voltage dependence of activation of Ca(v)2.1 channels toward more depolarized potentials, which may lead to loss of calcium channel activity. A similar depolarizing shift is reported for Ca(v)2.1 channels in leaner (Wakamori et al., 1998) and rolling Nagoya mouse neurons (Mori et al., 2000). However, the changes in *tg-4J* activation and inactivation kinetics appear to be unique to this particular tottering mutation. Finally, there was no profound change in the calcium current density in *tg-4J* or *Tg-5J*, unlike many of the mouse tottering mutations, including leaner (Lorenzon et al., 1998) (Dove et al., 1998) rolling Nagoya (Mori et al., 2000) and the two targeted alleles (Jun et al., 1999; Fletcher et al., 2001).

The voltage activation changes for the *tg-4J* homozygote from both the BHK transfected cells and the dissociated Purkinje cells show that both approaches can yield comparable results. Although we saw a similar trend in the *Tg-5J* heterozygote results, we were unable to complete this analysis by looking at the *Tg-5J* homozygotes because of their poor viability on the B10 background. Future studies using more robust homozygotes from the B10;BALB cross can potentially confirm the BHK results, hopefully without introducing confounding problems arising from the modified strain background. These two new tottering mouse models with altered calcium channel electrophysiology provide further opportunities to understand how perturbations in the Ca(v)2.1 calcium channel regulate neuronal excitation and its underlying association with the human disorders.

Abbreviations

BHK, baby hamster kidney
B6, B10, BALB, C3H and CAST, 5 inbred strains of mice
CACNA1A, calcium channel gene encoding the Ca(v)2.1 or P/Q-type subunit
CSD, cortical spreading depression
EA2, episodic ataxia type 2
EEG, electroencephalographic recordings
FHM, familial hemiplegic migraine
GFP, green fluorescent protein
het, heterozygous
N2, second backcross generation
SCA6, spinocerebellar ataxia type 6
tg, original mouse tottering allele
tg-4J, mouse tottering-4J allele
Tg-5J, mouse Tottering-5J allele
TH, tyrosine hydroxylase

Acknowledgements

This work was supported by NIH P40 RR01183 (SC), NS32801 (VL), and The Jackson Laboratory institutional shared services are supported by NIH CA34196. We thank Dr. J. Zhang for the GFP transgenic mice; Connie Birkenmeier, Zhong-wei Zhang and Robert Burgess for their expert advice.

References

Alonso I, Barros J, Tuna A, Seixas A, Coutinho P, Sequeiros J, Silveira I. A novel R1347Q mutation in the predicted voltage sensor segment of the P/Q-type calcium-channel alpha-subunit in a family with progressive cerebellar ataxia and hemiplegic migraine. Clin Genet 2004;65:70–72. [PubMed: 15032980]

Austin MC, Schultzberg M, Abbott LC, Montpied P, Evers JR, Paul SM, Crawley JN. Expression of tyrosine hydroxylase in cerebellar Purkinje neurons of the mutant tottering and leaner mouse. Brain Res Mol Brain Res 1992;15:227–240. [PubMed: 1279353]

Ayata C, Shimizu-Sasamata M, Lo EH, Noebels JL, Moskowitz MA. Impaired neurotransmitter release and elevated threshold for cortical spreading depression in mice with mutations in the alpha1A subunit of P/Q type calcium channels. Neuroscience 2000;95:639–645. [PubMed: 10670432]

Barrett CF, Cao YQ, Tsien RW. Gating deficiency in a familial hemiplegic migraine type 1 mutant P/Q-type calcium channel. J Biol Chem 2005;280:24064–24071. [PubMed: 15795222]

Beauvais K, Cave-Riant F, De Barace C, Tardieu M, Tournier-Lasserve E, Furby A. New CACNA1A gene mutation in a case of familial hemiplegic migraine with status epilepticus. Eur Neurol 2004;52:58–61. [PubMed: 15240985]

Catterall WA. Structure and regulation of voltage-gated Ca2+ channels. Annu Rev Cell Dev Biol 2000;16:521–555. [PubMed: 11031246]

Chattopadhyaya B, Di Cristo G, Higashiyama H, Knott GW, Kuhlman SJ, Welker E, Huang ZJ. Experience and activity-dependent maturation of perisomatic GABAergic innervation in primary visual cortex during a postnatal critical period. J Neurosci 2004;24:9598–9611. [PubMed: 15509747]

Chen C, Okayama H. High-efficiency transformation of mammalian cells by plasmid DNA. Mol Cell Biol 1987;7:2745–2752. [PubMed: 3670292]

Clark HB, Burright EN, Yunis WS, Larson S, Wilcox C, Hartman B, Matilla A, Zoghbi HY, Orr HT. Purkinje cell expression of a mutant allele of SCA1 in transgenic mice leads to disparate effects on motor behaviors, followed by a progressive cerebellar dysfunction and histological alterations. J Neurosci 1997;17:7385–7395. [PubMed: 9295384]

Cricchi F, Di Lorenzo C, Grieco GS, Rengo C, Cardinale A, Racaniello M, Santorelli FM, Nappi G, Pierelli F, Casali C. Early-onset progressive ataxia associated with the first CACNA1A mutation identified within the I–II loop. J Neurol Sci 2007;254:69–71. [PubMed: 17292920]

Dove LS, Abbott LC, Griffith WH. Whole-cell and single-channel analysis of P-type calcium currents in cerebellar Purkinje cells of leaner mutant mice. J Neurosci 1998;18:7687–7699. [PubMed: 9742139]

Fletcher CF, Lutz CM, O'Sullivan TN, Shaughnessy JD, Hawkes R, Frankel WN, Copeland NG, Jenkins NA. Absence epilepsy in tottering mutant mice is associated with calcuim channel defects. Cell 1996;87:607–617. [PubMed: 8929530]

Fletcher CF, Tottene A, Lennon VA, Wilson SM, Dubel SJ, Paylor R, Hosford DA, Tessarollo L, McEnery MW, Pietrobon D, Copeland NG, Jenkins NA. Dystonia and cerebellar atrophy in Cacna1a null mice lacking P/Q calcium channel activity. FASEB J 2001;15:1288–1290. [PubMed: 11344116]

Guida S, Trettel F, Pagnutti S, Mantuano E, Tottene A, Veneziano L, Fellin T, Spadaro M, Stauderman K, Williams M, Volsen S, Ophoff R, Frants R, Jodice C, Frontali M, Pietrobon D. Complete loss of P/Q calcium channel activity caused by a CACNA1A missense mutation carried by patients with episodic ataxia type 2. Am J Hum Genet 2001;68:759–764. [PubMed: 11179022]

Hamill OP, Marty A, Neher E, Sakmann B, Sigworth FJ. Improved patch-clamp techniques for high-resolution current recording from cells and cell-free membrane patches. Pflugers Arch 1981;391:85–100. [PubMed: 6270629]

Hans M, Luvisetto S, Williams ME, Spagnolo M, Urrutia A, Tottene A, Brust PF, Johnson EC, Harpold MM, Stauderman KA, Pietrobon D. Functional consequences of mutations in the human alpha1A calcium channel subunit linked to familial hemiplegic migraine. J Neurosci 1999;19:1610–1619. [PubMed: 10024348]

Herrup K, Wilczynski SL. Cerebellar cell degeneration in the leaner mutant mouse. Neuroscience 1982;7:2185–2196. [PubMed: 7145091]

Jeng CJ, Sun MC, Chen YW, Tang CY. Dominant-negative effects of episodic ataxia type 2 mutations involve disruption of membrane trafficking of human P/Q-type Ca2+ channels. J Cell Physiol 2008;214:422–433. [PubMed: 17654512]

Jouvenceau A, Eunson LH, Spauschus A, Ramesh V, Zuberi SM, Kullmann DM, Hanna MG. Human epilepsy associated with dysfunction of the brain P/Q-type calcium channel. Lancet 2001;358:801–807. [PubMed: 11564488]

Jun K, Piedras-Renteria ES, Smith SM, Wheeler DB, Lee SB, Lee TG, Chin H, Adams ME, Scheller RH, Tsien RW, Shin HS. Ablation of P/Q-type Ca(2+) channel currents, altered synaptic transmission, and progressive ataxia in mice lacking the alpha(1A)-subunit. Proc Natl Acad Sci U S A 1999;96:15245–15250. [PubMed: 10611370]

Jurman ME, Boland LM, Liu Y, Yellen G. Visual identification of individual transfected cells for electrophysiology using antibody-coated beads. Biotechniques 1994;17:876–881. [PubMed: 7840967]

Kaja S, van de Ven RC, Broos LA, Veldman H, van Dijk JG, Verschuuren JJ, Frants RR, Ferrari MD, van den Maagdenberg AM, Plomp JJ. Gene dosage-dependent transmitter release changes at neuromuscular synapses of CACNA1A R192Q knockin mice are non-progressive and do not lead to morphological changes or muscle weakness. Neuroscience 2005;135:81–95. [PubMed: 16111830]

Klöckner U, Mikala G, Varadi M, Varadi G, Schwartz A. Involvement of the carboxyl-terminal region of the α_1 subunit in voltage-dependent inactivation of the cardiac calcium channels. J Biol Chem 1995;270:17306–17310. [PubMed: 7615531]

Kraus RL, Sinnegger MJ, Koschak A, Glossmann H, Stenirri S, Carrera P, Striessnig J. Three new familial hemiplegic migraine mutants affect P/Q-type Ca(2+) channel kinetics. J Biol Chem 2000;275:9239–9243. [PubMed: 10734061]

Lindquist SG, Norremolle A, Hjermind LE, Hasholt L, Nielsen JE. Meiotic CAG repeat instability in spinocerebellar ataxia type 6: maternally transmitted elongation in a presumed sporadic case. J Neurol Sci 2006;241:95–98. [PubMed: 16310805]

Lorenzon NM, Lutz CM, Frankel WN, Beam KG. Altered calcium channel currents in Purkinje cells of the neurological mutant mouse leaner. J Neurosci 1998;18:4482–4489. [PubMed: 9614225]

Mori Y, Friedrich T, Kim MS, Mikami A, Nakai J, Ruth P, Bosse E, Hofmann F, Flockerzi V, Furuichi T, et al. Primary structure and functional expression from complementary DNA of a brain calcium channel. Nature 1991;350:398–402. [PubMed: 1849233]

Mori Y, Wakamori M, Oda S, Fletcher CF, Sekiguchi N, Mori E, Copeland NG, Jenkins NA, Matsushita K, Matsuyama Z, Imoto K. Reduced voltage sensitivity of activation of P/Q-type Ca2+ channels is associated with the ataxic mouse mutation rolling Nagoya (tg(rol)). J Neurosci 2000;20:5654–5662. [PubMed: 10908603]

Mullner C, Broos LA, van den Maagdenberg AM, Striessnig J. Familial hemiplegic migraine type 1 mutations K1336E, W1684R, and V1696I alter Cav2.1 Ca2+ channel gating: evidence for beta-subunit isoform-specific effects. J Biol Chem 2004;279:51844–51850. [PubMed: 15448138]

Niidome T, Teramoto T, Murata Y, Tanaka I, Seto T, Sawada K, Mori Y, Katayama K. Stable expression of the neuronal BI (class A) calcium channel in baby hamster kidney cells. Biochem Biophys Res Commun 1994;203:1821–1827. [PubMed: 7945334]

Noebels JL, Sidman RL. Inherited epilepsy: spike-wave and focal motor seizures in the mutant mouse tottering. Science 1979;204:1334–1336. [PubMed: 572084]

Ophoff RA, Terwindt GM, Vergouwe MN, van Eijk R, Oefner PJ, Hoffman SMG, Lamerdin JE, Mohrenweiser HW, Bulman DE, Ferrari M, Haan J, Lindhout DB, vOG-J B, Hofker MH, Ferrari MD, Frants RR. Familial hemiplegic migraine and episodic ataxia type-2 are caused by mutations in the Ca^{2+} channel gene CACNL1A4. Cell 1996;87:543–552. [PubMed: 8898206]

Pietrobon D, Striessnig J. Neurobiology of migraine. Nat Rev Neurosci 2003;4:386–398. [PubMed: 12728266]

Pulst SM, Santos N, Wang D, Yang H, Huynh D, Velazquez L, Figueroa KP. Spinocerebellar ataxia type 2: polyQ repeat variation in the CACNA1A calcium channel modifies age of onset. Brain 2005;128:2297–2303. [PubMed: 16000334]

Qian J, Noebels JL. Presynaptic Ca(2+) influx at a mouse central synapse with Ca(2+) channel subunit mutations. J Neurosci 2000;20:163–170. [PubMed: 10627593]

Rhyu IJ, Abbott LC, Walker DB, Sotelo C. An ultrastructural study of granule cell/Purkinje cell synapses in tottering (tg/tg), leaner (tg(la)/tg(la)) and compound heterozygous tottering/leaner (tg/tg(la)) mice. Neuroscience 1999a;90:717–728. [PubMed: 10218773]

Rhyu IJ, Oda S, Uhm CS, Kim H, Suh YS, Abbott LC. Morphologic investigation of rolling mouse Nagoya (tg(rol)/tg(rol)) cerebellar Purkinje cells: an ataxic mutant, revisited. Neurosci Lett 1999b; 266:49–52. [PubMed: 10336181]

Ruta V, Chen J, MacKinnon R. Calibrated measurement of gating-charge arginine displacement in the KvAP voltage-dependent K+ channel. Cell 2005;123:463–475. [PubMed: 16269337]

Shimazaki H, Takiyama Y, Sakoe K, Amaike M, Nagaki H, Namekawa M, Sasaki H, Nakano I, Nishizawa M. Meiotic instability of the CAG repeats in the SCA6/CACNA1A gene in two Japanese SCA6 families. J Neurol Sci 2001;185:101–107. [PubMed: 11311290]

Spacey SD, Hildebrand ME, Materek LA, Bird TD, Snutch TP. Functional implications of a novel EA2 mutation in the P/Q-type calcium channel. Ann Neurol 2004;56:213–220. [PubMed: 15293273]

Tokuda S, Kuramoto T, Tanaka K, Kaneko S, Takeuchi IK, Sasa M, Serikawa T. The ataxic groggy rat has a missense mutation in the P/Q-type voltage-gated Ca2+ channel alpha1A subunit gene and exhibits absence seizures. Brain Res 2007;1133:168–177. [PubMed: 17196942]

Tottene A, Fellin T, Pagnutti S, Luvisetto S, Striessnig J, Fletcher C, Pietrobon D. Familial hemiplegic migraine mutations increase Ca(2+) influx through single human CaV2.1 channels and decrease maximal CaV2.1 current density in neurons. Proc Natl Acad Sci U S A 2002;99:13284–13289. [PubMed: 12235360]

Uchitel OD, Protti DA, Sanchez V, Cherksey BD, Sugimori M, Llinás R. P-type voltage-dependent calcium channel mediates presynaptic calcium influx and transmitter release in mammalian synapses. Proc Natl Acad Sci USA 1992;89:3330–3333. [PubMed: 1348859]

van den Maagdenberg AM, Pietrobon D, Pizzorusso T, Kaja S, Broos LA, Cesetti T, Van de Ven RC, Tottene A, van der Kaa J, Plomp JJ, Frants RR, Ferrari MD. A Cacna1a knockin migraine mouse model with increased susceptibility to cortical spreading depression. Neuron 2004;41:701–710. [PubMed: 15003170]

Wakamori M, Hidaka H, Akaike N. Hyperpolarizing muscarinic responses of freshly dissociated rat hippocampal CA1 neurones. J Physiol 1993;463:585–604. [PubMed: 7504109]

Wakamori M, Yamazaki K, Matsunodaira H, Teramoto T, Tanaka I, Niidome T, Sawada K, Nishizawa Y, Sekiguchi N, Mori E, Mori Y, Imoto K. Single tottering mutations responsible for the neuropathic phenotype of the P-type calcium channel. J Biol Chem 1998;273:34857–34867. [PubMed: 9857013]

Wheeler DB, Randall A, Tsien RW. Roles of N-type and Q-type Ca2+ channels in supporting hippocampal synaptic transmission. Science 1994;264:107–111. [PubMed: 7832825]

Wu LG, Westenbroek RE, Borst JG, Catterall WA, Sakmann B. Calcium channel types with distinct presynaptic localization couple differentially to transmitter release in single calyx-type synapses. J Neurosci 1999;19:726–736. [PubMed: 9880593]

Xie G, Clapcote SJ, Nieman BJ, Tallerico T, Huang Y, Vukobradovic I, Cordes SP, Osborne LR, Rossant J, Sled JG, Henderson JT, Roder JC. Forward genetic screen of mouse reveals dominant missense mutation in the P/Q-type voltage-dependent calcium channel, CACNA1A. Genes Brain Behav 2007;6:717–727. [PubMed: 17376154]

Zhuchenko O, Bailey J, Bonnen P, Ashizawa T, Stockton DW, Amos C, Dobyns WB, Subramony SH, Zoghbi HY, Lee CC. Autosomal dominant cerebellar ataxia (SCA6) associated with small polyglutamine expansions in the α_{1A}-voltage-dependent calcium channel. Nature Genet 1997;15:62–69. [PubMed: 8988170]

Zwingman TA, Neumann PE, Noebels JL, Herrup K. Rocker is a new variant of the voltage-dependent calcium channel gene Cacna1a. J Neurosci 2001;21:1169–1178. [PubMed: 11160387]

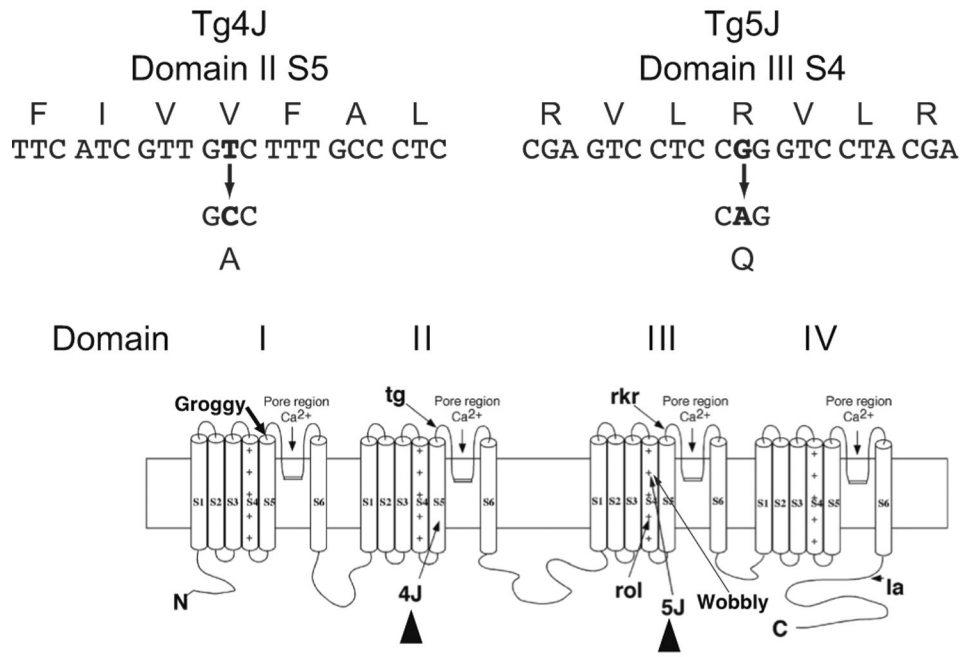

Figure 1. The *tg-4J* and *Tg-5J* mutations

The *tg-4J* had a thymine (T*)* to cytosine (C*)* transition at nucleotide position 1742, resulting in a valine (V)-to-alanine (A) switch. *Tg-5J* showed a guanine (G*)* to adenine (A*)* change at nucleotide 3755, changing an arginine (R)-to-glutamine (Q).

Below is the proposed transmembrane topography of the CACNA1A protein and the sites of the recessive mouse alleles, *Cacna1a*^{tg} (tottering), *Cacna1a*$^{tg\text{-}la}$ (leaner), *Cacna1a*^{rol} (rolling Nagoya*)*, and *Cacna1a*^{rkr} (rocker). The dominant wobbly mouse and the recessive groggy rat mutation sites are also included. Triangles highlight the position of the *tg-4J* and *Tg-5J* mutations.

High Voltage Calcium Channel	CACNA1A	KSL**R**VL**R**VL**R**PLKTIKRLPKL
	CACNA1B	KSL**R**VL**R**VL**R**PLKTIKRLPKL
Low Voltage Calcium Channel	CACNA1H	GVL**R**VL**R**LL**R**TL**R**PL**R**VISRA
Sodium Channel	SC10A	SGL**R**TF**R**VL**R**ALKTVSVIPGL

Figure 2. Conserved sequence with the arginine motif in ion-gated channels

Examples from ion-gated channels showing the conserved arginine motifs in bold. The sequence shown from each channel is identical between human, rat and mouse. The underlined R represents the arginine mutated in *Tg-5J*.

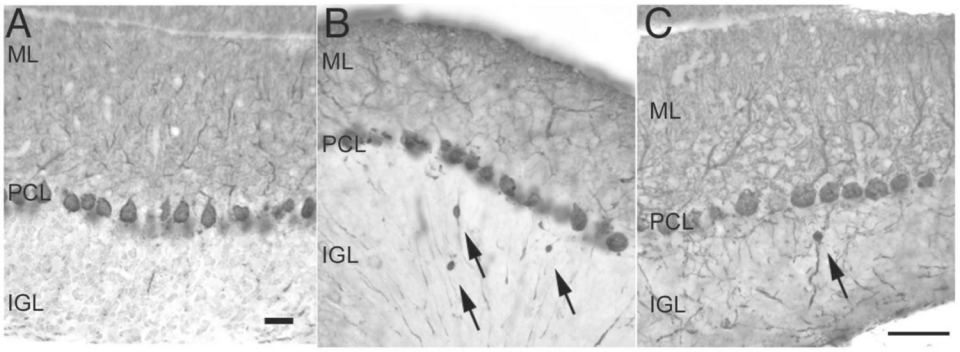

Figure 3. Calbindin staining in adult cerebellum

Calbindin staining in adult wild-type (A), *tg-4J* homozygous (B) and *Tg-5J* heterozygous (C) cerebellum reveals axonal swellings of the Purkinje cell axons (arrows) in the internal granule cell layer of the *tg-4J* and *Tg-5J* mutants. Scale bars 25μM.

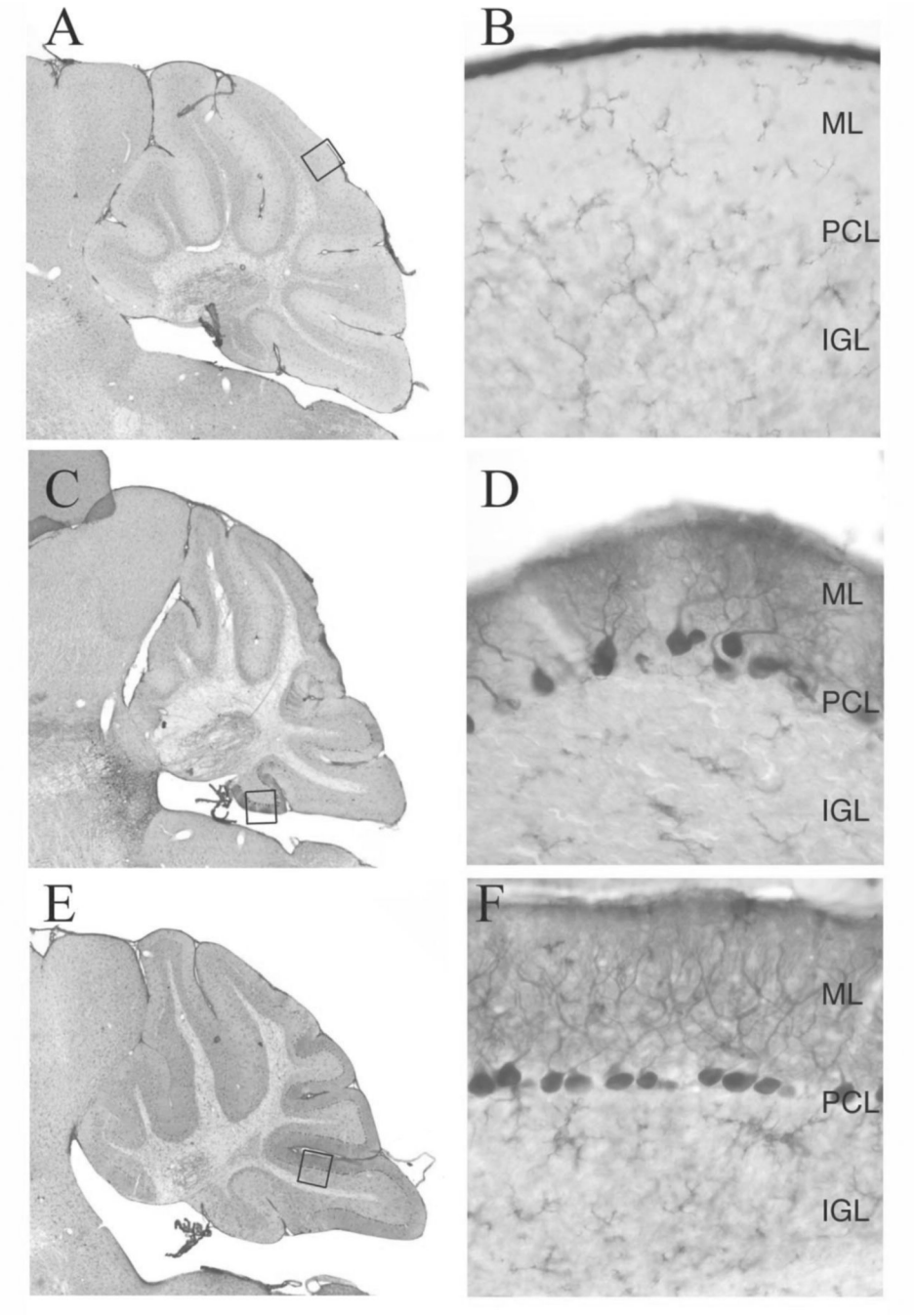

Figure 4. Tyrosine hydroxylase expression in the cerebellum

Tyrosine hydroxylase staining in the cerebellum from control (A,B), *tg-4J* (C,D) and *Tg-5J* het. (E,F) adult animals reveal persistent TH expression in subpopulations of Purkinje cells from both the *tg-4J* and *Tg-5J* animals. Abbreviations: Purkinje (PCL), molecular (ML), internal granule cell layer (IGL) (Location of higher magnification pictures shown as dashed box).

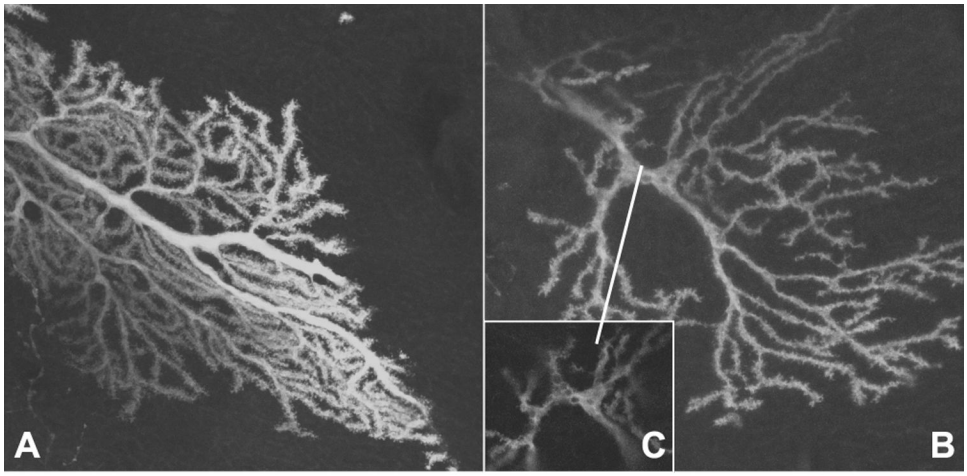

Figure 5. Green Fluorescent protein labeling of Purkinje cells from the *Tg-5J* homozygote

Confocal microscopy of a GFP labeled Purkinje cell from (A) control aged 24 days and (B) *Tg-5J* homozygote at 24 days. Panel C highlights the abnormal vacuoles observed within the primary branch of the *Tg-5J* mutant.

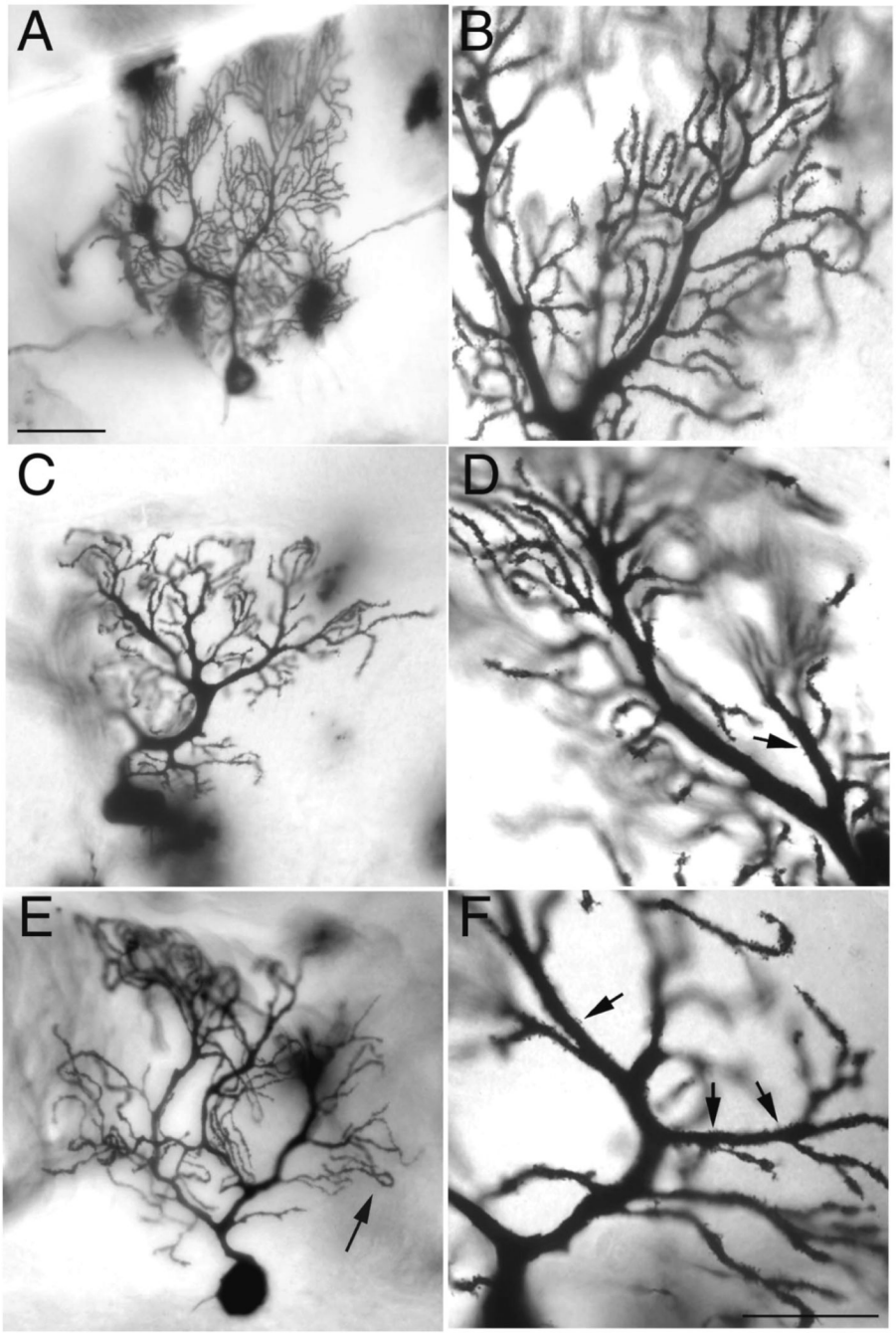

Figure 6. Golgi impregnation of individual cerebellar Purkinje cells shows dendritic abnormalities in adult *tg-4J* and *Tg-5J* mutants of over 1 year of age

Branching in the wild-type Purkinje cell appears very dense with increasing number of branching points near the distal tips (A, B). In *tg-4J* homozygous mutants a slight thickening of primary dendrites and ectopic spines is observed (C, D). *Tg-5J* heterozygous mutants show a decrease in branching and have down turned distal ends of their dendritic tree and ectopic spines shown by the arrows (E and F). Scale bars 50uM (A, C, and E) and 25uM (B, D, and F).

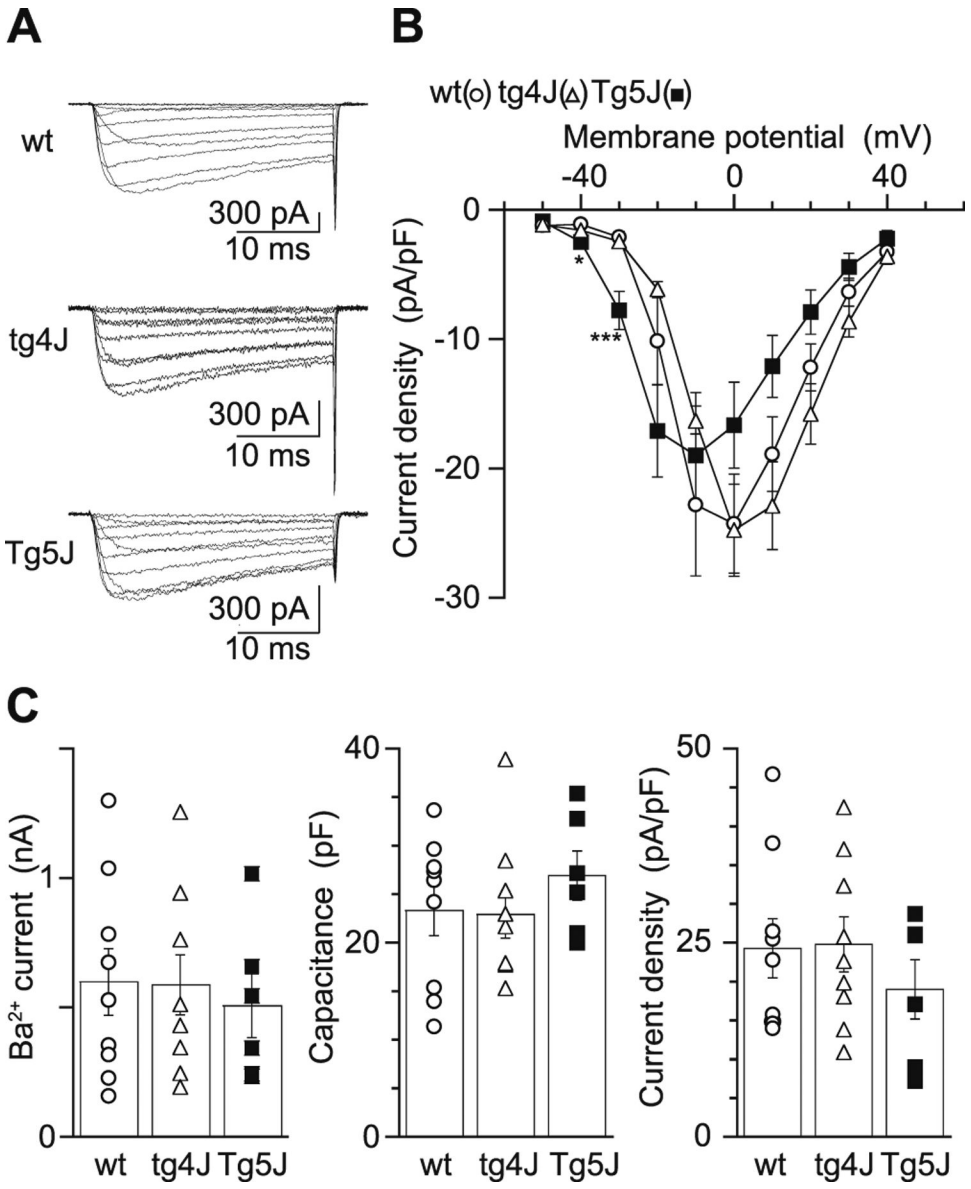

Figure 7. Comparison of Ba2+ currents in BHK cells expressing the mutant and the wild-type Ca (v)2.1 channels

A, Families of Ba^{2+} currents evoked by 30-msec depolarizing pulses from −50 to 40 mV for the wild-type Ca(v)2.1 channel (top), the *tg-4J* Ca(v)2.1 channel (middle) and the *Tg-5J* Ca(v) 2.1 channel (bottom) with 10-mV increments from a holding potential (V_h) of −100 mV.

B, Current density was plotted against membrane potential. Each point represents an average value of 8, 9 and 6 BHK cells expressing the wild-type Ca(v)2.1 channel (open circle), the *tg-4J* Ca(v)2.1 channel (open triangle) and the *Tg-5J* Ca(v)2.1 channel (filled square), respectively.

C, Distribution of peak current amplitude (left), cell capacitance (middle), and current density (right). Individual values of Ca^{2+} channel currents in the wt, the *tg-4J* mutant and the *Tg-5J* mutant Ca(v)2.1 channels and their means (open box) ± S.E. are shown. Error bars indicate mean ± S.E. if they are larger than symbols. **P* < 0.05 and ****P* <0.001 versus wt.

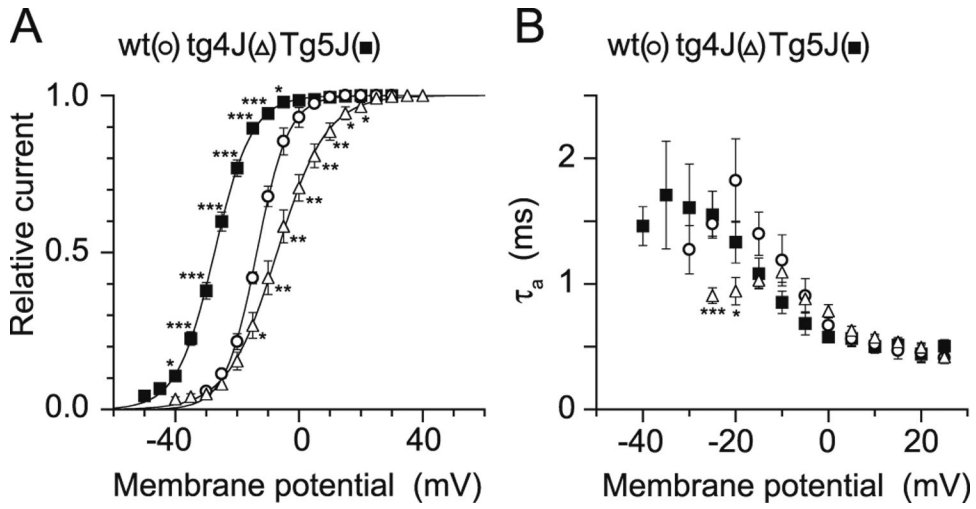

Figure 8. Ca(v)2.1 activation currents in wild-type, *tg-4J* and *Tg-5J*

A, Amplitudes of tail currents were normalized to the maximal tail current amplitude. The mean values from 5 BHK cells of the wild-type Ca(v)2.1 channel, 7 BHK cells of the *Tg-5J* Ca(v)2.1 channel and 6 BHK cells of the *tg-4J* Ca(v)2.1 channel were plotted against test pulse potentials and fitted to the Boltzmann equation with a midpoint ($V_{0.5}$) of −14.5 mV and a slope factor (*k*) of 5.1 mV for the wild-type Ca(v)2.1 channel (open circle), and a $V_{0.5}$ of −27.3 mV and a *k* of 6.1 mV for the *Tg-5J* Ca(v)2.1 channel (filled square) and a $V_{0.5}$ of −7.0 mV and a *k* of 7.8 mV for the *tg-4J* Ca(v)2.1 channel (open triangle).

B, Comparison of activation kinetics. Activation time constants were obtained from single-exponential fits of activation phase during 5-msec depolarizing steps. Data are expressed as mean ± SE of 6, 5 and 5 BHK cells expressing the wild-type, the *Tg-5J* and the *tg-4J* Ca(v)2.1 channels, respectively.

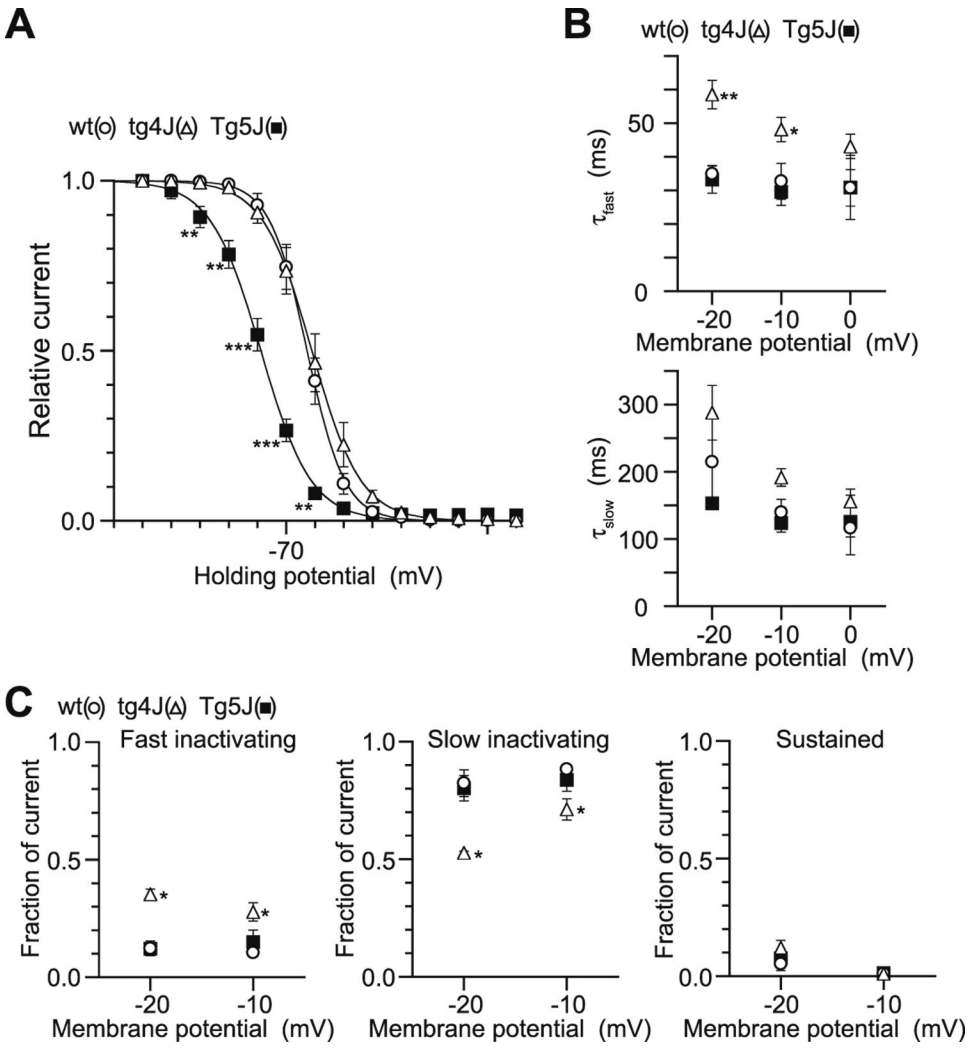

Figure 9. Ca(v)2.1 inactivation curves in wild-type, *tg-4J* and *Tg-5J*

A, Amplitudes of currents evoked by the test pulses were normalized to the current amplitude induced by the test pulse after a 2-sec V_h replacement of −120 mV. The mean values from 6 BHK cells expressing the wild-type Ca(v)2.1 channel (open circle), 5 BHK cells expressing the *Tg-5J* channel (filled square) and 5 BHK cells expressing the *tg-4J* channel (open triangle) were plotted as a function of potentials of the 2-sec V_h displacement, and were fitted to the Boltzmann equation. $V_{0.5}$ and k were −63.1 and 6.3 mV for the wild-type α1A channel, −79.0 and 8.6 mV for the *Tg-5J* channel and −61.2 and 7.7mV for the *tg-4J* channel, respectively. B and C, Current decay was fitted by a sum of two exponential functions. The mean inactivation time constants, τ_{fast} (top) and τ_{slow} (bottom), were plotted as a function of test potentials from −20 to 0 mV. The fractions of the components, fast (left), slow inactivation (middle), and sustained components (right), were plotted against test potentials. Data are expressed as mean ± SE of 3, 6 and 3 BHK cells expressing the wild-type, the *Tg-5J* and the *tg-4J* Ca(v)2.1 channels, respectively. Error bars indicate mean ± SE if they are larger than symbols.

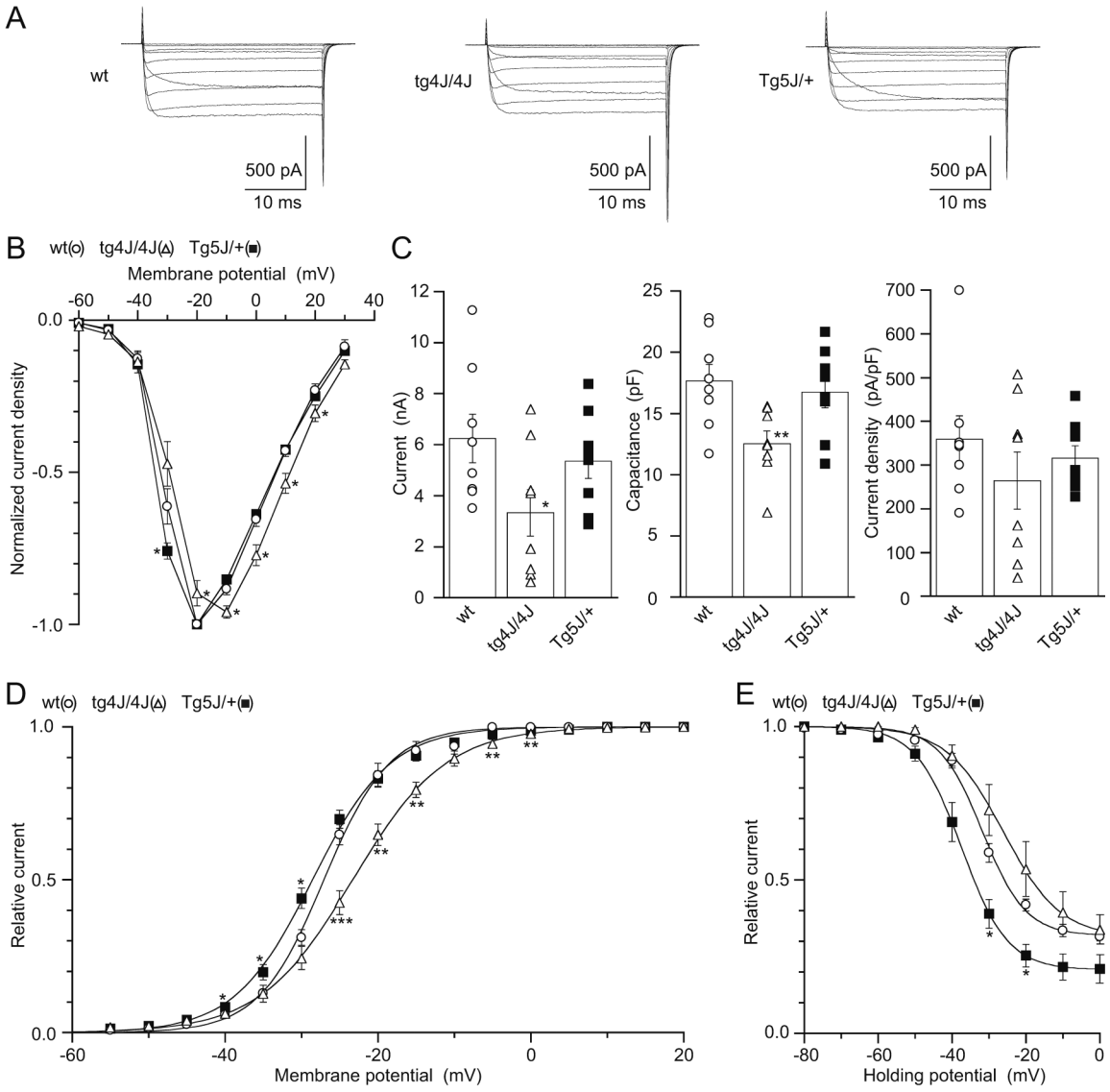

Figure 10. Comparison of Ca(v)2.1 currents recorded in cerebellar Purkinje cells dissociated from wild-type, *tg-4J /tg-4J* homozygotes and *Tg-5J/+* heterozygous mice

A, Families of Ba^{2+} currents evoked by 30-msec depolarizing pulses from −60 to 30 mV for wt, *tg-4J /4J*, and *Tg-5J/+* mice with 10-mV increments from a V_h of −80 mV. B, Normalized current density was plotted against membrane potential. Each point represents an average value of 8 Purkinje cells from the wt (open circle), *tg-4J /4J* (filled triangle) and *Tg-5J/+* (open square), respectively.

C, Distribution of peak current amplitude (left), cell capacitance (middle), and current density (right). Individual values of Ca^{2+} channel currents in wt, *tg-4J /4J* and *Tg-5J/+* Purkinje cells and their means (open box) ± S.E. are shown.

D, Activation curves. Amplitudes of tail currents were normalized to the maximal tail current amplitude. The mean values from 7 wt, *7 tg-4J /4J*, and 8 *Tg-5J/+* Purkinje cells were plotted against test pulse potentials and fitted to the Boltzmann equation.

E, Inactivation curves. Amplitudes of currents evoked by the test pulses were normalized to the current amplitude induced by the test pulse after a 2-sec V_h replacement of −80 mV. The mean values from 3 wt, 3 *tg-4J /4J*, and 6 *Tg-5J/+* were plotted as a function of potentials of

the 2-sec V_h displacement, and were fitted to the Boltzmann equation. Error bars indicate mean ± S.E. if they are larger than symbols. *$P < 0.05$, **$P < 0.01$ and ***$P < 0.001$ versus wt.

Table 1

Activation and inactivation parameters of Ca(v)2.1 channels in BHK cells and dissociated Purkinje cell neurons.

BHK cells	**Activation parameters**[1)]				**Inactivation parameters**[2)]			
	$V_{0.5}$	**SE**	***k***	**SE**	$V_{0.5}$	**SE**	***k***	**SE**
wt	−14.49	1.01	5.06	0.46	−63.05	1.85	−6.27	0.63
tg4J	−7.03	1.63 **	7.67	0.37 **	−61.16	2.86	−7.66	0.25
Tg5J	−27.29	0.63 ***	6.07	0.38 **	−79	1.75 ***	−8.56	0.57

Purkinje neurons	**Activation parameter**[1)]				**Inactivation parameters**[3)]					
	$V_{0.5}$	**SE**	***k***	**SE**	***a***	**SE**	$V_{0.5}$	**SE**	***k***	**SE**
wt	−26.86	0.69	4.31	0.35	0.68	0.01	−31.79	0.84	−5.81	0.15
tg4J/4J	−23.35	1.03 *	5.95	0.27 ***	0.69	0.03	−25.45	3.72	−7.27	0.85
Tg5J/+	−28.48	0.61	5.03	0.44	0.79	0.05	−37.3	1.24 *	−5.74	0.67

Abbreviations: *k* is the slope factor.

[1)] $V_{0.5}$, the half-maximal activation

[2)] $V_{0.5}$, the half-maximal inactivation

[3)] *a*, the rate of inactivating component and $V_{0.5}$, the half-inactivation potential

* $P < 0.05$

** $P < 0.01$

*** $P < 0.001$ versus wt